Geochimica et Cosmochimica Acta 389 (2025) 74–83

Contents lists available at ScienceDirect

Geochimica et Cosmochimica Acta

journal homepage: www.elsevier.com/locate/gca

Adsorption pathways of boron on clay and their implications for boron cycling on land and in the ocean

Simon J. Ring [a,b,*], Michael J. Henehan [a,c], Roberts Blukis [d], Friedhelm von Blanckenburg [a,b]

[a] Earth Surface Geochemistry, Deutsches GeoForschungsZentrum GFZ, 14473 Potsdam, Germany
[b] Freie Universität Berlin, Institute of Geological Sciences, 14195 Berlin, Germany
[c] School of Earth Sciences, University of Bristol, Wills Memorial Building, Queens Road, Bristol BS8 1RJ, United Kingdom
[d] Leibniz-Institut für Kristallzüchtung, 12489 Berlin, Germany

ARTICLE INFO

Associate Editor: Nathalie Vigier

Keywords:
Boron isotopes
Clay
Adsorption
Surface complexation model
Boron cycle

ABSTRACT

Reversible adsorption and isotope fractionation of boron on the surface of clay minerals is a key process that impacts boron isotope cycling in porewater, rivers and the ocean. However, the differences in boron isotope fractionation factors between various clay minerals and their dependence on fluid chemistry are not well known. We performed two sets of experiments, using solutions of pure water with added boron and seawater, to explore the isotope behavior during adsorption of boron onto kaolinite, smectite and illite. We found that the amount of sorbed boron increases with ionic strength of solutions and is proportional to the cation exchange capacity of a given clay mineral. Maximum adsorption is observed in alkaline seawater, which we attribute to the efficient fixation of magnesium-borate ion pairs onto negatively charged surface sites. Isotopic fractionation is modestly different between clays and demonstrates that clay surfaces preferentially sorb borate, even when the concentration of borate in solution is low. In both pure water and seawater, adsorbed complexes retain the isotopic composition of their dissolved precursors (borate or boric acid) with minimal isotopic fractionation. In other words, isotopic composition of adsorbed boron is set by the ability of clays to adsorb boron from an already fractionated boron pool rather than specific fractionation associated with the complexation reaction. Our experimental results allow us to provide revised constraints on the adsorbed boron being transported in terrestrial fluids and the ocean.

1. Introduction

The isotope ratio of boron (expressed as $\delta^{11}B = (({}^{11}B/{}^{10}B_{sample})/({}^{11}B/{}^{10}B_{standard}) - 1) \times 1000$) dissolved in surface waters is relevant to several proxy applications. On the continents, rivers integrate the products of rock weathering reactions that are associated with strong isotopic fractionation, such that the $\delta^{11}B$ of riverine boron can be used to identify basin-scale changes in weathering regimes (Noireaux et al., 2021; Ercolani et al., 2019; Lemarchand & Gaillardet, 2006). In the oceans, planktonic foraminifera coprecipitate seawater boron into their calcite shell with isotopic fractionation that depends on ambient pH. The $\delta^{11}B$ of fossil calcite thus allows for the reconstruction of the past carbonate system, provided that the $\delta^{11}B$ of seawater is known (Foster and Rae, 2016). In both applications, a key mechanism that sets fluid $\delta^{11}B$ is the reversible adsorption of boron onto the surface of minerals that are present in soils, rivers and the ocean.

Among the most common of these minerals are clays, such as kaolinite, smectite and illite. Clays are sheet silicate minerals comprising layers of octahedrally coordinated metal cations (Al, Mg, Fe) flanked by tetrahedrally coordinated silicate, with individual platelets as the most common growth habit. While oxygen at the external basal surfaces of the platelet is fully incorporated in bridging tetrahedra or octahedra, those on the edge surface are not. Edge surfaces are hence covered by reactive hydroxyl groups where complexation reactions can take place (Keren and Talpaz, 1984). Depending on the pH of the surrounding fluid, the charge state of edge hydroxyl groups can be positive ($>OH_2^+$), neutral ($>OH$) or negative ($>O^-$). In the same way, when boron is dissolved in water, the degree to which it is hydroxylated also depends on fluid pH (Fig. 1). At acidic conditions, three hydroxyl groups coordinate boron in a planar-trigonal geometry to form neutral boric acid ($B(OH)_3$), whereas most boron is present as a tetrahedral borate anion ($B(OH)_4$) when pH is above 9 (Fig. 1). It follows that the degree to which boron is able to

* Corresponding author.
E-mail address: simon.ring@gfz-potsdam.de (S.J. Ring).

https://doi.org/10.1016/j.gca.2024.08.014
Received 7 December 2023; Accepted 14 August 2024
Available online 21 August 2024

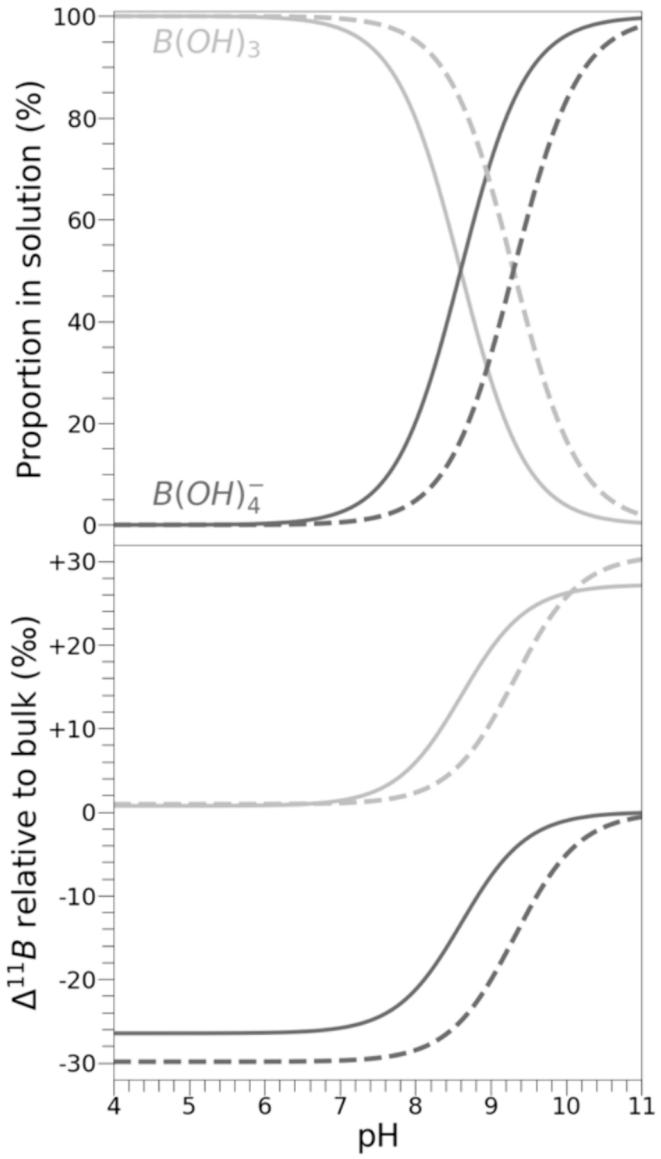

Fig. 1. Borate speciation in water (top) and its impact on isotope composition (bottom). Solid and dashed lines represent speciation in seawater and pure water (respectively), which differ in their fractionation factor (Klochko et al., 2006) and equilibrium constant (Hershey et al., 1986). At low pH (<7), $B(OH)_3$ is the dominant species, so its $\delta^{11}B$ is equivalent to the bulk $\delta^{11}B$, defined as the sum of $B(OH)_3$ and $B(OH)_4^-$. The same is true for $B(OH)_4^-$ at high pH (>10).

approach and complex to the surface of clay minerals at a given pH will reflect the competing impact of pH on boron speciation and the charge of available reactive sites. Previous experimental experiments, conducted at elevated ionic strength, have shown that the adsorbed concentration of boron is highest in mildly alkaline water and diminishes when pH approaches more alkaline or acidic conditions (Hingston, 1964; Mattigod et al. 1985; Goldberg et al., 1993; Keren et al., 1981; Goldberg and Glaubig, 1986; Su and Suarez, 1995).

$B(OH)_3$ and $B(OH)_4^-$ differ in their respective $\delta^{11}B$ values by 26.0 to 27.2 ‰ (Fig. 1; Klochko et al., 2006; Nir et al., 2015). Boron isotope fractionation can thus arise not only from specific fractionation associated with a given reaction but also if the reaction is selective for one boron species at a pH value where its isotopic composition is different from the bulk composition. For example, at a fluid pH of 8, adsorption of $B(OH)_4^-$ with a minor positive fractionation would result in a light $\delta^{11}B$ of adsorbed boron with a $\Delta^{11}B$ of −15 ‰. Equally, the same adsorbed $\delta^{11}B$ could be achieved by adsorption and significant negative fractionation of $B(OH)_3$, the most abundant species at these conditions (Fig. 1). Considering both the amount and isotopic composition of adsorbed boron over a wide range of pH values, where the speciation of aqueous borate is known (Fig. 1), makes it possible to distinguish between both scenarios and elucidate the mechanism by which boron attaches to the clay surface.

Few studies have so far investigated the isotope behavior during adsorption on clays. Schwarcz et al. (1969) first found that seawater became more enriched in ^{11}B following contact with illite, and speculated that adsorption to sediment in estuaries is the main cause for the heavy $\delta^{11}B$ of the modern ocean (39.61 ± 0.04 ‰; Foster et al., 2010). Adsorption experiments on Mississippi delta suspended sediment subsequently confirmed the preferential fixation of the lighter ^{10}B isotope at a seawater pH of 8 (Spivack et al., 1987). When pH was further reduced to 7, the amount of sorbed boron was found to decrease, whereas the magnitude of fractionation increased (Palmer et al., 1987). Similar results have also been determined for the adsorption of boron on soil clays (Lu et al., 2024). To explain this pattern, Palmer et al. (1987) proposed an empirical model in which aqueous $B(OH)_3$ and $B(OH)_4^-$ are adsorbed by river sediments at a given pH with characteristic partition coefficients (1.68 and 7.82, respectively) and fractionation factors (0.969 and 0.992, respectively).

However, river sediments vary widely in their constituent components (such as clay minerals, organic matter, quartz and feldspar) which likely differ in their ability to adsorb and fractionate boron. For example, iron and manganese oxyhydroxides can fix large amounts of boron with a light $\delta^{11}B$ (Lemarchand et al. 2007) while adsorption on quartz is presumably negligible due to its small surface area. There is therefore little reason to assume that the isotopic fractionation associated with adsorption on bulk sediment from the Mississippi delta (Spivack et al., 1987; Palmer et al., 1987) is representative of all rivers. Relatedly, because Mississippi delta sediment is a mixture of many minerals, it is difficult to extrapolate these findings to rivers whose mineral assemblages differ. This, together with the lack of isotope studies at lowionic strength, means that the size and isotopic composition of the boron pool present on clay surfaces is still unknown, hampering modeling of local and global boron cycling (e.g., Noireaux et al., 2021; Lemarchand et al., 2002a).

Here we aim to constrain the interaction of clay minerals with dissolved boron by performing a new set of adsorption experiments at high and low ionic strength on three different clay types. The results allow for a more refined characterization of the boron being transported in the hydrosphere.

2. Methods

2.1. Clay pretreatment

We obtained kaolinite (KGa-1b), smectite (SWy-3) and illite (IMt-2) source clays originally distributed by the Clay Minerals Society. Because these source clays were mined from geologic deposits, they contain impurities and minor amounts of sorbed ions. Clays were therefore pretreated to obtain mineralogically pure samples with a consistent particle size distribution (2—–0.2 μm) and unoccupied reactive surface sites. Specifically, clay powder was placed in a 15 ml polypropylene centrifuge tube and filled with 10 ml of buffered surfactant, consisting of buffered 3.3 M sodium hexametaphosphate ($Na_6P_6O_{18}$) to facilitate the deagglomeration of particles. Suspended particles were separated according to particle size by centrifugation following Stoke's Law (Poppe et al., 2001) assuming specific densities of 2.1 g/cm^3 for smectite and 2.6 g/cm^3 for kaolinite and illite (Totten et al., 2002). The suspension containing particles within 2—–0.2 μm was then extracted and dried in an oven at 60 °C for at least 12 h. Chipera and Bish (2001) found, using X-ray diffraction (XRD), that this size separation yields clay samples with a mineralogical purity (f_{clay}) of 95 % or more. XRD patterns obtained for our pretreated samples using a STOE StadiP X-ray

diffractometer (Supplementary Material) confirm a high purity of illite (f_{clay} of 95 %) and kaolinite (f_{clay} of 100 %). However, our smectite samples still contained about 25 % of quartz. We use these values as corrections when we quantify the partition coefficient (see below).

A final pretreatment was required to remove adsorbed contaminants from the refined clay samples. Exactly 400 mg of the dried clay powder was weighed and transferred into a new 15 ml polypropylene centrifuge tube. We then repeatedly mixed clay with 10 ml of ultrapure Milli-Q water, centrifuged the suspension at high speed (2600 × g) for 10 min and carefully decanted the solution. Preliminary measurements suggested that ten such rinses in Milli-Q water were sufficient to remove the vast majority of adsorbed boron from clay surfaces (Supplementary Material).

2.2. Experimental set-up

For the sorption experiments, we prepared two stock solutions representing high and low ionic strength endmembers: (*i*) artificial seawater made by dissolving laboratory-grade salts in Milli-Q water (Table 1), and (*ii*) a solution (termed 'pure water' from here on), which had the same boron content as seawater but lacked any other dissolved ions. In both cases, dissolved boron was derived by addition of NIST-SRM 951a boric acid standard, resulting in a solution $\delta^{11}B$ of 0.08 ‰ (±0.16 ‰, 2σ; $n = 8$) for seawater and −0.04 ‰ (±0.05 ‰, 2σ; $n = 4$) for pure water.

The 400 mg pretreated clays were immersed in 10 ml of either seawater or pure water, and the pH of each solution was adjusted by adding small amounts of 1.0 M NaOH or distilled 1.0 M HCl. Previous studies concluded that boron adsorption requires as little as 2 h to reach stoichiometric equilibrium (Mezuman and Keren, 1981; Hingston, 1964). We conducted further tests to constrain the timescale for isotopic equilibrium, which showed that solution $\delta^{11}B$ values settled to constant values approximately 24 h after mixture with clay minerals (Supplementary Material). For adsorption experiments, pretreated clays were continually agitated in a reciprocal rotator for at least 48 h at a constant temperature of 21 °C (±1 °C). Afterwards, the suspension was centrifuged at high speed (2600*g*) for 10 min and 2 ml of clear sample solution was drawn for analysis. The pH of the remaining solution was immediately measured using a hand-held ProfiLine (pH 3110) glass–ceramic electrode that was regularly calibrated against NIST-certified buffers.

Previous studies raised the possibility that clay minerals could partly dissolve in suspension and subsequently reprecipitate as various secondary phases. For example, Zhang et al. (2021) performed adsorption experiments similar to ours and concluded that the dissolution of kaolinite had triggered the formation of saponite out of solution. Secondary phases tend to incorporate significant amounts of boron so their precipitation would obscure the effect of boron adsorption in our experiments. However, kinetics of dissolution-precipitation reactions are generally slow at low temperature (e.g., Köhler et al., 2003). In the case of Zhang et al. (2021), oversaturation with respect to saponite (saturation index above 1) was only reached after 7 days, whereas experiments presented in this study were terminated after exactly 48 h. The short duration of our experiments likely does not permit significant recrystallization, and we assume that the boron chemistry of the fluid is primarily influenced by fast adsorption reactions with the clay surface.

Table 1
Recipe for the preparation of 1 kg of artificial seawater, adopted from Millero (2013).

Salt	Mass (g)
NaCl	24.8780
$MgCl_2$	5.2121
Na_2SO_4	4.1566
$CaCl_2$	1.1828
KCl	0.7237
$NaHCO_3$	0.1496
KBr	0.1039
$B(OH)_3$	0.0266
$SrCl_2$	0.0149
NaF	0.0030

2.3. Chemical analysis

We measured the boron concentration and isotopic values of each sample solution and compared them to the composition of the original seawater or pure water stock solutions to characterize the adsorption process under differing solution pH. All measurements were performed at the Helmholtz Laboratory for the Geochemistry of the Earth Surface (HELGES) in Potsdam, Germany.

Boron concentrations in seawater samples were measured using a *ThermoFisher iCAP* TQ-ICP-MS. Sample aliquots were diluted in 0.5 M HNO_3 by a factor of 600 to avoid excessive plasma loading by Na and saturation of Faraday cups. Along with samples, we measured five solutions of OSIL standard Atlantic seawater (Millero et al., 2008) which were diluted in 0.5 M HNO_3 by factors of 600, 632, 667, 706 and 750 as a calibration. 30 µL of rhodium (~50 µmol/kg) solution was added to each sample as an internal standard to correct for instrumental mass drift. Machine reproducibility (±8 µmol/kg, 2σ) was assessed through repeated measurements of seawater from the Gulf of Eilat as an in-house standard.

Boron concentrations in pure water were measured using a *ThermoFisher Neptune* MC-ICP-MS. Samples were diluted in 0.5 M HNO_3 by a factor of 225 and measured against NIST 951a with concentrations between 15 and 20 ppb as a calibration. Machine reproducibility (±8 µmol/kg, 2σ) was assessed through repeated measurement of ERM-AE121 (Vogl and Rosner, 2011).

Boron isotope ratios were measured using a *ThermoFisher Neptune* MC-ICP-MS. Samples were each purified beforehand by passing buffered aliquots (approximately 15 ng of boron) through a microcolumn containing 20 µL of Amberlite IRA 743 anion-exchange resin (Lemarchand et al., 2002b), which was subsequently rinsed with 1600 µL of Milli-Q water. The boron sample was eluted with 840 µL of 0.5 M HNO_3. This yielded purified samples with a boron concentration of 9 – 20 ppb, with elution tails containing, on average, 11 pg of boron. For isotope ratio measurements, samples, along with ERM-AE121 as a consistency standard, were bracketed with a 20 ppb solution of NIST SRM 951a boric acid standard to convert raw isotope ratios to the $\delta^{11}B$ notation. ^{11}B and ^{10}B isotopes were collected in H3 and L3 cups (respectively), both equipped with 10^{13} Ω amplifiers. Procedural blanks contained around 17 pg of boron, such that the average magnitude of blank-correction on samples amounted to 0.04 ‰ in $\delta^{11}B$ and never exceeded 0.12 ‰. We related machine reproducibility to signal intensity of each sample through separate measurements of purified NIST RM 8301 (Foram) standard. These yielded an average $\delta^{11}B$ of 14.58 ‰ (±0.45 ‰, 2σ; $n = 49$) across a ^{11}B intensity range from 6 – 417 mV (Supplementary Material), in good agreement with the inter-laboratory average value (14.51 ± 0.17 ‰, 2σ) presented by Stewart et al. (2020).

2.4. Parameter estimation

We can infer the extent of adsorption reactions as the concentration ([B]) and mass bias-corrected isotope ratios (R) of the dissolved boron pool are known before and after the experiment. We characterize the mass and fractionation of adsorbed boron in each samples by calculating a nondimensional partition coefficient (K_D) and fractionation factor (α_B):

$$K_D = \frac{[B]_{adsorbed}}{[B]_{dissolved}} \text{ and}$$

$$\alpha_B = \frac{R_{adsorbed}}{R_{dissolved}}.$$

$[B]_{dissolved}$ and $R_{dissolved}$ were directly measured, while $[B]_{adsorbed}$ and $R_{adsorbed}$ were calculated from the differences in the absolute mass (M) and R of dissolved boron before and after contact with pretreated clay minerals:

$$[B]_{adsorbed} = \frac{M_{before} - M_{after}}{0.4g \times f_{clay}},$$

$$R_{adsorbed} = \frac{M_{before} \times R_{before} - M_{after} \times R_{after}}{M_{before} - M_{after}}.$$

Uncertainties in K_D and α_B were propagated through Monte Carlo subsampling ($n = 5000$) of $[B]_{dissolved}$ and $R_{dissolved}$ within their respective measurement errors.

3. Results

In pure water, K_D for all three clay minerals is low (<4), meaning that the concentration of boron adsorbed on the mineral surface is not much higher than the concentration of boron in solution (Fig. 2). Additionally, adsorption on all clay minerals appears to be insensitive to pH (Fig. 2). In contrast, isotopic fractionation of adsorbed boron features a clear pH dependence. Most samples have α_B of 0.981—0.992, but the adsorbed fraction approaches the composition of the dissolved boron pool ($\alpha_B \sim 1$) beginning at a pH of > 8.5, when boron speciation is dominated by $B(OH)_4^-$ (Fig. 1).

In seawater, K_D is generally higher and subject to a more pronounced dependence on the pH of the solution (Fig. 3). There is a modest increase in K_D when pH is raised from 3 to 7, followed by more rapid increase once seawater reaches alkaline conditions above a pH of 8. At a pH of 9, K_D values are between two to four times higher than at low pH and reach a maximum in each clay mineral. Isotopic fractionation factors are similar to those in pure water at a circumneutral and alkaline pH but, unlike results for pure water, again approach a α_B of 1 at acidic pH (Fig. 3). This yields an α_B pattern with a distinct minimum within the pH range of the modern ocean interior (Lauvset et al., 2016).

In both our experiment sets, these general patterns are common to all three minerals we investigated. However, absolute values of K_D and α_B of each mineral are modestly offset from each other. At most pH values, smectite adsorbs the most and fractionates the least, while illite and kaolinite are marked by a lower capacity for adsorption but a more pronounced fractionation (Figs. 2 and 3).

4. Discussion

4.1. Controls on boron adsorption

Variations in concentration and isotopic composition of aqueous B $(OH)_3$ and $B(OH)_4^-$ are similar in pure water and seawater (Fig. 1), yet adsorption behavior clearly differs between both fluids (Figs. 2 and 3). It follows that clay minerals do not merely adsorb boron according to its speciation in solution alone, but that adsorption must be influenced by additional controls related to the composition of the fluid.

Previous studies found that under high concentrations of Na^+ or low concentrations of Ca^{2+} (I>0.05), boron partitioning to clay surfaces is maximized at a pH of around 8.5 and is reduced at other pH values, resulting in a parabolic adsorption envelope (Fig. 4; Goldberg et al., 1993; Hingston, 1964; Su and Suarez, 1995; Mattigod et al., 1985). To explain this pattern, Keren and Mezuman (1981) proposed that clay surface sites have a high affinity to $B(OH)_4^-$ but that adsorption is inhibited at low and high pH due to the low abundance of $B(OH)_4^-$ and competition with free OH^-, respectively. In other words, complexation might inherently favor one boron species, even when speciation in the fluid is dominated by another (Fig. 1).

Furthermore, the parabolic dependence of K_D on pH is diminished when ionic strength is reduced (Fig. 4) and eventually approaches the uniform K_D found in our pure water experiments ($I \approx 0$). This implies that the stability of underlying surface sites to which boron is complexing is modulated by the ionic strength. Charged surface sites in particular ($>OH_2^+$ or $>O^-$, depending on pH) will attract solvated charges of opposite sign in the form of an electric double layer, the establishment of which comes at an entropic cost. In pure water, this cost is high as the double layer can only be composed of polarized water molecules. At high ionic strength, in turn, compensation of charges is easier, and the cost is lower due to the abundance of available counterions which can be incorporated in the electric double layer.

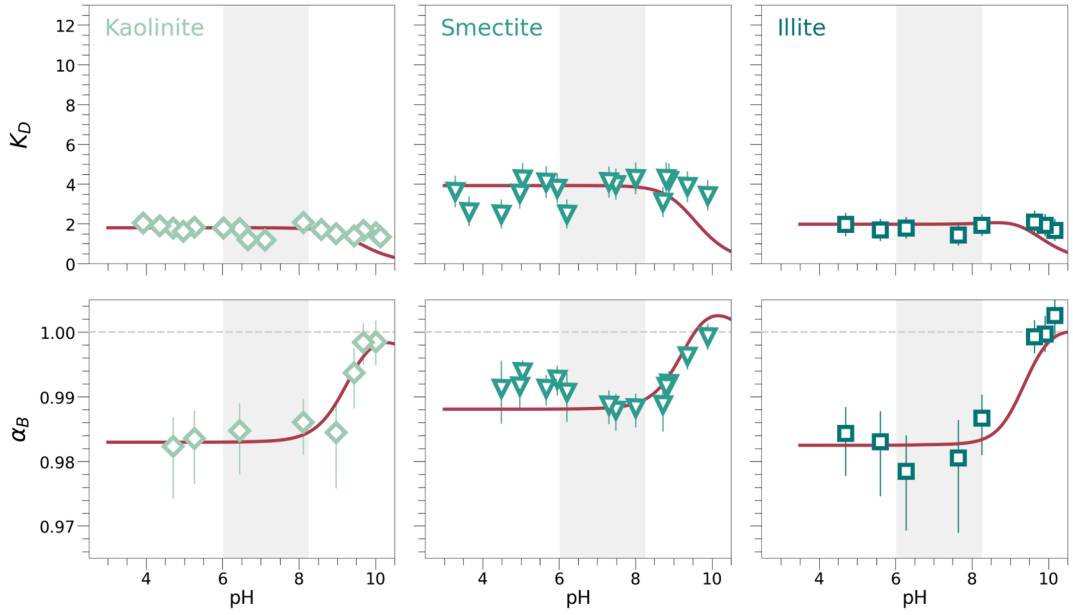

Fig. 2. The partition coefficient (K_D; **top row**) and isotope fractionation factor (α_B; **bottom row**) of adsorbed boron on KGa-1b kaolinite, SWy-3 smectite and IMt-2 illite in pure water, where the plotted uncertainties represent the propagated 95% confidence interval. The results of surface complexation models with the best fit are shown in red (see Section 4.1). Vertical grey bars represent the range of median annual pH values in global rivers.

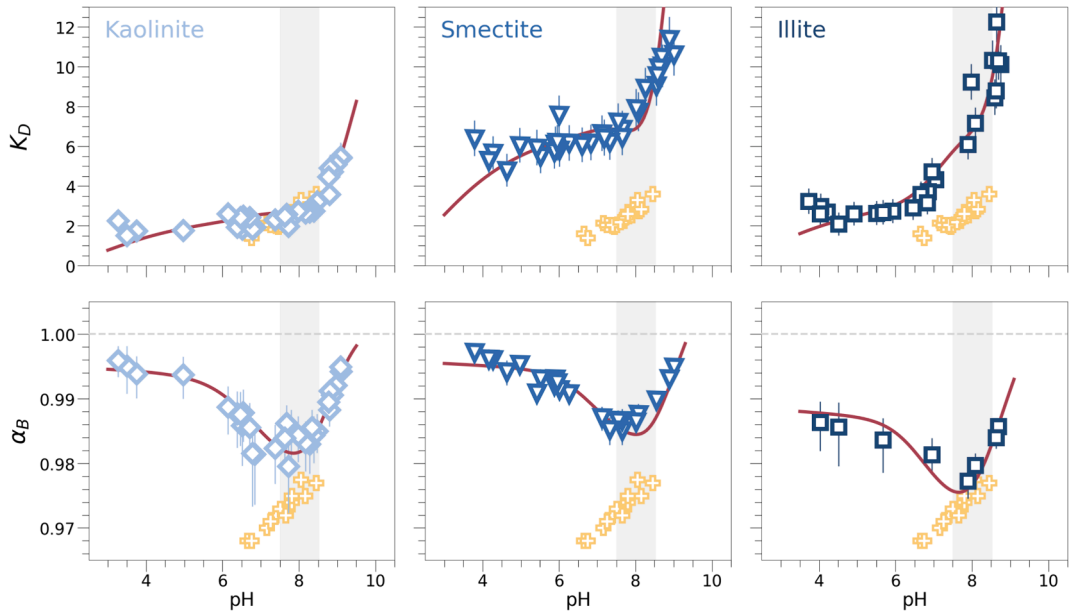

Fig. 3. Same as Fig. 2, but for adsorption in seawater. Here, vertical grey bars represent the range of pH values in the modern ocean (Lauvset et al., 2016). Orange crosses show data for Mississippi delta sediments (Palmer et al., 1987).

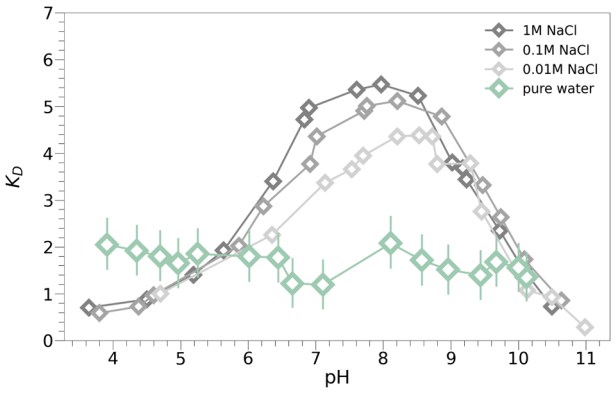

Fig. 4. Published boron adsorption envelopes for kaolinite in NaCl solutions (recalculated from Goldberg et al., 1993) compared to adsorption in pure water (this study). In NaCl solutions a distinct maximum in adsorption appears around a pH of 8.5. However, the maximum is reduced at lowered concentrations of dissolved Na^+, and disappears when all solutes, other than boron, are absent from solution. Note that Goldberg et al. (1993) used KGa-2 kaolinite with a higher density of crystal defects than the KGa-1b kaolinite used in this study.

Formation and stabilization of charged surface sites might therefore be facilitated by the presence of dissolved ions.

Finally, our seawater results (I=0.7) do not match the parabolic K_D pattern found in previous experiments where a similar ionic strength was emulated by addition of NaCl (Goldberg et al., 1993; Su and Suarez, 1995). Instead, we find that K_D in seawater shows a rapid increase when pH is elevated above 8, meaning that boron adsorption is also sensitive to the elemental makeup of the surrounding solution. Cations in particular can ionically bond to aqueous $B(OH)_4^-$, meaning that a certain fraction of $B(OH)_4^-$ exists in the form of ion pairs. In NaCl solutions, the only ion pair is neutral $NaB(OH)_4$, but in seawater the presence of divalent cations means that there are ion pairs with a net positive charge, such as $MgB(OH)_4^+$ or $CaB(OH)_4^+$. Positively charged ion pairs would readily complex to deprotonated surface sites ($>O^-$) which would otherwise be inaccessible to unpaired $B(OH)_4^-$ (Mattigod et al., 1985).

In summary, existing experimental data suggests that there are three separate controls on boron adsorption: speciation of the boron in solution, the character of mineral surface sites and the ionic composition of the fluid. To elucidate the relative roles of these controls in setting our experimental results, we fitted our results to a surface complexation model with a diffuse double layer using PHREEQC v3.7.3 (Parkhurst and Appelo, 2013) and the Pitzer thermodynamic database. The Pitzer database includes ion pairing between $B(OH)_4^-$, Ca^{2+} and Mg^{2+} in solution has also been noted as the most appropriate database for fluids with a high ionic strength (Farmer et al., 2019).

4.2. *Surface complexation modeling*

The model describes the complexation reactions to a mineral surface and takes into account the electrical properties of the surrounding diffusive double layer. Formation constants were optimized by randomly varying them (n = 1000) within a broad range and selecting the combination of parameters providing the closest fit (highest coefficient of determination) to the experimental results. We assume that adsorption occurs at the amphoteric sites at the plate edges (Keren and Taipaz, 1984). Site density is set to a reference concentration of 2.31 sites/nm^2 (Davis and Kent, 1990) distributed over the specific surface areas of each clay obtained from N_2-BET (Dogan et al., 2006, 2007). We note that this might be subject to bias as the area of plate edges is necessarily smaller than the full surface area. In addition, the accessibility of clays to N_2 in a partial vacuum is not identical to the accessibility of the same clays to ions in suspension, such that N_2-BET may not adequately reflect the available surface area. Cation exchange capacity (CEC) would be a more appropriate measure but converting CEC (in meq/g) to a surface area (in m^2/g) is difficult. We therefore opt to use published N_2-BET values, which are proportional to CEC in our studied clay minerals (Borden and Giese, 2001; Kahle and Stamm, 2007), but we maintain that absolute modelled constants consequently need to be used with caution.

We find experimental features in both pure water and seawater can be reasonably replicated in a surface complexation model by two to three complexation reactions (red curves in Figs. 2, 3 and summarized in Fig. 5): specifically, reactions of (*i*) $B(OH)_3$ with protonated surface sites and (*ii*) $B(OH)_4^-$ with neutral surface sites. Both of these reactions are consistent with ATR-FTIR measurements (Su & Suarez, 1995). In addition, we assume that (*iii*) positively charged ion pairs between $B(OH)_4^-$

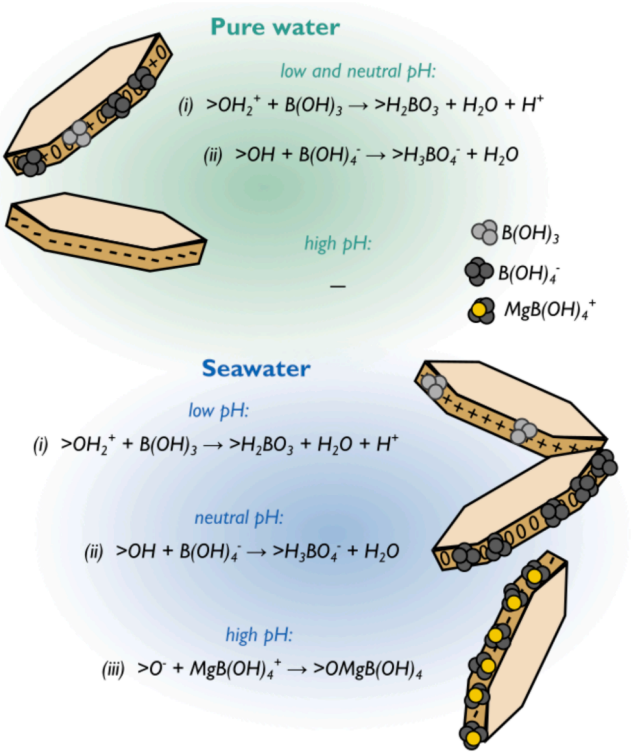

Fig. 5. Proposed models of boron adsorption in pure water and seawater, using reactions consistent with ATR-FTIR measurements (Su & Suarez, 1995). Differences in ionic strength between both solutions impact adsorption behavior at a given pH by changing the surface charge state and enabling the pairing of B $(OH)_4^-$ to a divalent cation like Ca^{2+} or Mg^{2+}.

and a divalent cation are able to attach to deprotonated surface sites (Mattigod et al., 1985). Clay edges become increasingly deprotonated at high pH, making them inaccessible to unpaired $B(OH)_4^-$ due to electrostatic repulsion and suppressing boron adsorption. Excluding reaction (*iii*) from our model would produce a parabolic pH-dependence in all clay minerals (Supplementary Material), similar to that seen for many other minerals when adsorption occurs in a NaCl solution (Fig. 4; Gaillardet and Lemarchand, 2018). Ion pairing between $B(OH)_4^-$ and a divalent cation thus appears necessary for the model to reproduce the increase in K_D observed in alkaline conditions. This is also consistent with measurements of the dissolved magnesium concentration, which show a reduction at a pH of > 7.5 (Supplementary Material). In reality, B $(OH)_4^-$ will pair with both magnesium and calcium but for convenience we restrict the model to adsorption of $MgB(OH)_4^+$ only. Magnesium is about five times as abundant as calcium in seawater and is more prone to associate with negative surface sites due to its higher charge density.

The modeled affinity of clay surfaces towards a given complexation reaction is quantified as an equilibrium constant (log K in Table 2), which expresses if boron is more likely to remain in solution (log K<0) or partition to the surface (log K>0). Inferred equilibrium constants are much larger for reaction (*ii*) than reaction (*i*) in both pure water and seawater (Table 2), which would be consistent with an inner-sphere association of $B(OH)_4^-$ and a looser outer-sphere association of $B(OH)_3$ to the mineral surface. Our results support the hypothesis that clay minerals preferentially adsorb $B(OH)_4^-$ (Keren and Mezuman, 1981). Adsorption in general is associated with an enthalpic penalty as it involves the fixation of a previously free molecule to a surface. As a charged ion, aqueous $B(OH)_4^-$ is surrounded by a layer of ordered water molecules. This coordination shell is released once $B(OH)_4^-$ complexes to a reactive surface site, which partially compensates the enthalpic penalty of adsorption. We speculate that this would make adsorption of B $(OH)_4^-$ more favorable than adsorption of neutral $B(OH)_3$ which, due to a lack of charge, will have a more loosely bound hydration shell.

Table 2
Parameters (equilibrium constants and fractionation factors) used to produce the surface complexation model fits shown in Figs. 2 and 3. Suffixes (s) and (aq) describe solid and aqueous states, respectively.

	Kaolinite		Smectite		Illite	
Surface reaction	log K	α*	log K	α*	log K	α*
$>OH_{(s)} + H^+_{(aq)} \rightarrow >OH^+_{2(s)}$	4.70	–	4.55	–	4.45	–
$>OH_{(s)} \rightarrow >O^-_{(s)} + H^+_{(aq)}$	−7.25	–	−7.50	–	−7.85	–
Pure water						
(*i*) $> OH^+_{2(s)} + B(OH)_{3(aq)} \rightarrow >H_2BO_{3(s)} + H_2O_{(aq)} + H^+_{(aq)}$	−3.29	0.995	−2.98	0.996	−3.18	0.997
(*ii*) $> OH_{(s)} + B(OH)_4^-{}_{(aq)} \rightarrow >H_3BO_4^-{}_{(s)} + H_2O_{(aq)}$	4.52	0.995	4.35	0.997	4.26	0.999
Seawater						
(*i*) $> OH^+_{2(s)} + B(OH)_{3(aq)} \rightarrow >H_2BO_{3(s)} + H_2O_{(aq)} + H^+_{(aq)}$	−3.07	0.995	−2.70	0.996	−2.86	0.989
(*ii*) $> OH_{(s)} + B(OH)_4^-{}_{(aq)} \rightarrow >H_3BO_4^-{}_{(s)} + H_2O_{(aq)}$	3.44	0.995	3.34	0.997	3.44	0.999
(*iii*) $> O^-_{(s)} + MgB(OH)_4^+ \rightarrow >MgB(OH)_{4(s)}$	2.21	1.002	2.75	1.004	3.04	1.003

*relative to $B(OH)_3$ in reaction (*i*) and $B(OH)_4^-$ in reactions (*ii*) and (*iii*).

In any case, the similarity of equilibrium constants across clay minerals (Table 2) demonstrates that the behavior described above is common to all of them. It furthermore follows that the inter-clay differences in K_D seen in this study (Figs. 2 and 3) and others (e.g., Keren and Mezuman, 1981; Goldberg and Glaubig, 1986), mainly arise from differences in physical properties, such as the available edge area, and not from the chemical reactivity of each clay.

The only notable mismatch between model and experimental data occurs in pure water at high pH (Fig. 2), where the model predicts a decline in K_D. Experimentally determined K_D values in pure water, while low, do not show such a decline and instead suggest that clays continue to adsorb small amounts of $B(OH)_4^-$ under these conditions (Fig. 2). In our view, this likely points to inaccuracies in our chosen protolysis constants (Table 2). Protolysis constants control how readily the mineral surface accepts or rejects protons from solution, but absolute published values for clay minerals vary significantly (Tertre et al., 2006; Bradbury & Baeyens, 1997, 2009; Gu et al., 2010; Liu et al., 2018; Motta and Miranda, 1989; Gu and Evans, 2008; Hao et al., 2019). One way to reconcile model output and data would be if the deprotonation constant prescribed in our model to each clay mineral (Table 2) is somewhat lower in pure water than it is in seawater (Hao et al., 2019). This would allow the mineral surface to remain neutral (>OH) at a high pH and enable complexation of $B(OH)_4^-$ (Fig. 5; Table 2).

Most isotope data is fit well with minimal specific fractionation during adsorption (α_B of 1.003 to 0.995). The only exception is $B(OH)_3$ adsorbed on illite, which, according to our modelling results, would have to be more fractionated (α_B of 0.989) to fit observed α_B values (Table 2). Complexes formed during reactions (*i–iii*) are monodentate and thus have the same coordination as the dissolved boron species, so there would be little reason to expect strong isotopic fractionation. In this regard our results differ from experimental studies on humic acid, birnessite and goethite (Lemarchand et al 2005; 2007) which explained α_B values through the formation of bidentate boron complexes, i.e., the bonding of boron to the mineral surface via two ligands instead of one. A bidentate association involves steric straining and a change in the coordination of boron. This results in large isotopic fractionation (<0.980; Lemarchand et al., 2007), analogous to the fractionation between B $(OH)_3$ and $B(OH)_4^-$ in solution. Bidentate complexes on clays are consistent with ATR-FTIR data (Su and Suarez, 1995) but they do not

need to be invoked to explain our α_B data, which can instead be explained if the $\delta^{11}B$ of adsorbed boron is minimally altered from its dissolved precursor.

The model also does not include other complexation reactions such as the adsorption of $B(OH)_4^-$ on $>OH_2^+$ sites. That is not to say that that these reactions cannot occur but rather that additional reactions are not necessary to explain our experimental results. For example, if the complexation of $B(OH)_4^-$ onto $>OH_2^+$ were a key process, we would expect adsorption in acidic seawater to result in pronounced isotope fractionation as $B(OH)_4^-$ isotopically light at these conditions. In contrast, experiments show that α_B approaches 1 when pH is below 5 (Fig. 3). To include this complexation reaction in the model would require us to assume a large specific (positive) isotope fractionation, which is hard to justify given the lack of steric straining. Instead, our model provides a parsimonious interpretation of the available observations with the smallest number of surface reactions. Our study improves on previous works by including boron isotopes as a constraint in complexation modeling. This allows us to place more confidence on our interpretation over modeling that is solely based on the amounts of boron being adsorbed.

Lastly, when calculating α_B from our surface complexation model results, we assume that the $\delta^{11}B$ of $MgB(OH)_4^+$ is not distinguishable from the $\delta^{11}B$ of unpaired $B(OH)_4^-$. However, we also note that reaction (*iii*), in contrast to reactions (*i*) and (*ii*), is associated with a positive specific fractionation (Table 2). An alternative possibility is therefore that $MgB(OH)_4^+$ may instead be isotopically heavier than $B(OH)_4^-$ by 4 ‰ or more, and that the specific fractionation during its adsorption is closer to those of the other reactions, i.e., slightly negative. Recent quantum chemical modeling indeed suggests that ion pairs are isotopically heavier than unpaired $B(OH)_4^-$ (Yin et al., 2023) but with a magnitude of fractionation (<1 ‰) that is too small to account for our modeling results.

4.3. Implications for dissolved riverine $\delta^{11}B$ as a weathering proxy

Boron is liberated in the critical zone on Earth's surface by dissolution of primary bedrock minerals and eventually transferred to rivers and the ocean. During this transfer, weathering reactions (such as secondary mineral formation) and uptake by vegetation in the soil can induce significant enrichment in ^{11}B within fluids (Cividini et al., 2010), meaning that the degree to which the boron conveyed to rivers is isotopically fractionated is a function of the weathering regime (Mao et al., 2019). The $\delta^{11}B$ measured in the *dissolved load* of streams is thus a useful tool to assess the prevalence of weathering reactions at a basin scale.

One complication is that an unknown fraction of the boron released in the critical zone will be present as an isotopically fractionated *adsorbed load* on the surface of particles. Thus, the $\delta^{11}B$ of the dissolved load depends on the fraction adsorbed and does not necessarily reflect what we term the *total load* (i.e., the sum of dissolved and adsorbed boron).

In most stream settings, where the mass ratio between fluid and solid is high ($\gg$1), K_D values determined in this study imply that less than 1 % of total boron is adsorbed on clay minerals. This is consistent with the results of Ercolani et al. (2019) and means that measuring the riverine dissolved $\delta^{11}B$ yields a close approximation of total $\delta^{11}B$, as adsorption is not able to significantly fractionate the much larger dissolved boron pool. Conversely, in environments where the ratio of fluid to solid is low (<1), such as soil pore spaces, adsorbed boron will comprise a larger portion of the total boron pool. Obtaining constraints on the composition of adsorbed boron is therefore necessary to determine the boron isotope budget in the subsurface.

For example, Noireaux et al. (2021) presented measurements of boron concentration and $\delta^{11}B$ for multiple reservoirs (bedrock, groundwater, soil sediments, etc.) at the Shale Hills critical zone observatory to identify major processes affecting boron cycling during soil formation. They inferred that the $\delta^{11}B$ of groundwater can be explained if > 70 % of boron released during weathering is adsorbed or incorporated on solid phases at a α_B of 0.979 ($\pm$0.002). We can again test the viability of these numbers using our new experimental data (Fig. 2). Pore waters at Shale Hills have a pH of 7, a mass ratio between fluid and solid of approximately 0.07 and a soil assemblage consisting of 40 % illite, 2 % kaolinite, 1 % iron oxides and 57 % non-adsorbing phases (Noireaux et al., 2021). Together with the relevant experimental K_D and α_B data for clay minerals (this work) and goethite (Lemarchand et al., 2007), mass balance predicts that 95 % of released boron at Shale Hills should be adsorbed onto solid particles with a net fractionation of 0.975, close to the observational requirements by Noireaux et al. (2021).

Note though that the boron isotope composition measured in porewaters will also be influenced through the uptake of boron by plants, which are an important component in the soil assemblage. Boron concentration in plant organic matter is high (>1000 μmol/kg; Geilert et al., 2015), so, depending on the productivity of the ecosystem, vegetation can be a significant terrestrial reservoir for boron. The bulk isotope composition of vegetation-bound boron appears to be identical to that present in soils (Xiao et al., 2022), but the $\delta^{11}B$ of various plant compartments, such as roots and leaves, spans a wide range of up to 30 ‰ (Roux et al., 2022). Isotope effects on the dissolved boron load can therefore arise if the boron pool in any of these plant compartments changes in size. For instance, the decay of a large amount of leaf litter and the associated release of isotopically heavy boron would increase the $\delta^{11}B$ of the rivers flowing within the catchment. A comprehensive quantification of organic fluxes will therefore be necessary to determine the contribution of plants to the riverine $\delta^{11}B$ and disentangling it from inorganic weathering processes like the adsorption on clays.

4.4. Surficial boron fluxes revisited

River water and suspended clay particles will eventually be transported to the global ocean, where they play a dual role in the boron cycle. The riverine dissolved load, in addition to the much smaller adsorbed load stored on riverine particles (see Section 4.2), is the biggest input of boron into ocean (Lemarchand et al., 2002a). On the other hand, riverine sediment will adsorb large amounts of marine boron once it has entered the estuary, due to the elevated K_D (Fig. 3) and the high boron concentration of seawater (416 μmol/kg) compared to river water (0.9 μmol/kg; average value in Lemarchand et al., 2002a). Determining the net role of rivers and their relative importance in setting seawater $\delta^{11}B$ compared to other fluxes, such as seafloor alteration, therefore requires a close budgeting of fluxes within the boron cycle (Lemarchand et al., 2002a; Schlesinger and Vengosh, 2016).

At present, rivers discharge about 35×10^3 km^3 of freshwater and 17×10^{12} kg of suspended sediment per year (Cohen et al. 2022; Li et al., 2020; Ghiggi et al., 2021; Syvitski et al., 2022), the latter of which is estimated to be composed of 15 % clay minerals, 2 % iron oxyhydroxides, 0.1 % manganese oxyhydroxides and 83 % non-adsorbing phases (Müller et al., 2021; Gibbs, 1977). Our experimental results, in combination with existing data (Lemarchand et al., 2007), allow us to revise the mass and composition of boron being transported in association with continental discharge to the ocean.

To this end, we compile a river database (n = 107; Fig. 6) containing, where available, freshwater discharge and suspended sediment fluxes (Cohen et al., 2022), median annual pH (UNEP GEMStat; https://www.gemstat.org), dissolved boron concentrations and $\delta^{11}B$ values (Lemarchand et al., 2002a; Ercolani et al., 2019; Liu et al., 2012) and the XRD-based clay mineral assemblage. We calculate that discharged clays have a flux-weighted average assemblage (Fig. 6) dominated by smectite (37 %) and illite (32 %), with minor amounts of kaolinite (19 %) and chlorite (12 %). Although estimating mineralogical abundances using XRD is associated with a large uncertainty, it is notable that the clay mineral distribution of surface sediments in the modern ocean also suggest a predominance of illite and smectite over kaolinite and chlorite

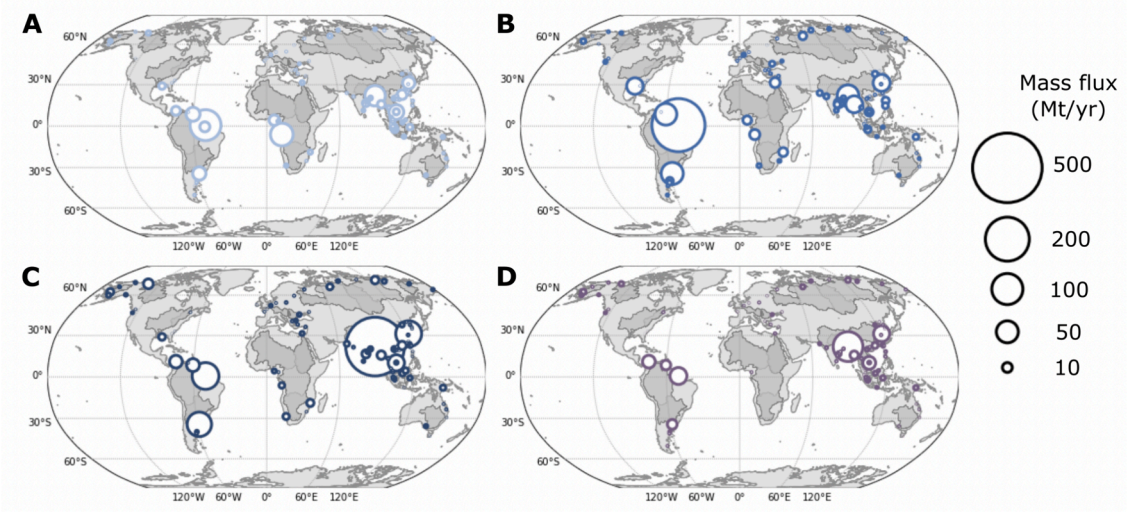

Fig. 6. Mass fluxes of the principal clay minerals kaolinite (A), smectite (B), illite (C) and chlorite (D) transported in globally distributed rivers (n = 107). Values are based on compiled XRD abundances of clays, an average clay fraction of 15 % in sediments and suspended sediment mass modelled in WBMsed (Cohen et al., 2022). Major river drainage basins are shown in grey.

in most basins (Griffin et al., 1968; Fagel, 2007). We interpret the agreement between our database and independent seafloor measurements to mean that the available data manages to capture the global-scale assemblage of riverine clay.

While they are suspended in river water (pH=7.0), we predict that sediments, including clays and metal oxyhydroxides, transport around 0.5×10^8 mol/yr of adsorbed boron with a light $\delta^{11}B$ of −10.1 ‰. As discussed in Section 4.2, this is dwarfed by the global dissolved load, which exceeds the adsorbed boron flux in rivers by three orders of magnitude and has a $\delta^{11}B$ of 10.8 ‰ (Table 2). Once the same sediments enter the ocean (pH=7.9), the concentration of adsorbed boron on their surface abruptly increases by a factor of > 100 and they are thus able to fix more than 83×10^8 mol/yr of marine boron at a $\delta^{11}B$ of 12.2 ‰ (Table 2).

Previous estimates of the boron adsorption flux in the global ocean were based on experiments using Mississippi delta sediments (Palmer et al., 1987; Spivack et al., 1987), which yielded a lower K_D and a more pronounced α_B than we found for clays (Fig. 3). A likely reason for this difference is that Mississippi delta sediments, in addition to clay minerals, are composed of other minerals with a broad range of adsorption behaviors. Coatings of iron oxyhydroxide on the sediment, for instance, will lead to boron adsorption with an intense isotope fractionation (Lemarchand et al., 2007), while the presence of any non-adsorbing phases, such as quartz, will dilute the average concentration of boron adsorbed on the sediment. Together, iron oxyhydroxides and quartz could bias α_B and K_D towards lower values (respectively) compared to those determined in this study, where all minerals except clays are excluded.

Despite the large differences in adsorption parameters (Fig. 3), accounting for the relative roles of riverine minerals, as we do in our revised estimate, does not yield substantially different results for the global adsorption flux of boron in the ocean. Our calculated mineral discharge rates and experimental parameters imply an adsorption flux close in magnitude and isotopic composition to that given by Lemarchand et al. (2002a), where single sedimentary K_D and α_B values were assumed (Table 3). The fact that both approaches produce similar results again suggests that the adsorption parameters of Palmer et al. (1987) represent the combined properties of many different minerals but also that suspended sediment from the Mississippi River is fortuitously similar in its mineral content to globally averaged sediment discharge. Together these calculations confirm that clastic sediments are able to bind a mass of boron equivalent to, at most, 40 % of the dissolved riverine input (Table 3).

Table 3
Composition and magnitude estimated for global boron fluxes.

	This study		Lemarchand et al. (2002a)	
	Mass (10^8 mol/yr)	$\delta^{11}B$ (‰)	Mass (10^8 mol/yr)	$\delta^{11}B$ (‰)
Dissolved	300.9–383.8[a]	10.8	351	10
Adsorbed (rivers)	0.4–0.6[b]	−10.1	–	–
Adsorbed (ocean)	82.8–121.1[b]	12.2	120	15

[a] based on the range of freshwater runoff (Cohen et al. 2022; Li et al., 2020; Ghiggi et al., 2021; Syvitski et al. 2022).
[b] based on the range of continental sediment export (Cohen et al. 2022; Li et al., 2020; Syvitski et al. 2022).

A subordinate role for boron adsorption contradicts early assumptions that adsorption onto terrigenous particles is the principal driver in setting seawater $\delta^{11}B$ by re-adsorbing the majority of riverine boron (Schwarcz et al., 1969; Harriss, 1969). Our result instead fit into more recent reviews which underscore the likely dominance of ocean crust as a fractionated boron sink (Lemarchand et al., 2002a; Simon et al., 2006). The significance of this is observation is nevertheless hard to assess since all fluxes are associated with unquantified but potentially large uncertainty, as can be seen in the case of the dissolved input (Table 3). Constraining these uncertainties more rigorously in the future would help produce more robust models of past and present boron cycling.

5. Conclusions

We present an improved quantification of the K_D and α_B associated with adsorption of boron onto the most common clay minerals in two solutions with high and low ionic strength. Our results differ from previous estimates (Palmer et al., 1987) insofar as they suggest a higher adsorbed boron concentration and lower isotopic fractionation. Isotope behavior in particular seems to be consistent with a propensity of all clays to adsorb $B(OH)_4^-$ without significant specific fractionation during attachment to the surface, as is invoked for adsorption on other substrates (Lemarchand et al., 2005; 2007). The presence of dissolved ions can mediate the accessibility of the clay surface to boron by stabilizing charged surface sites ($>OH_2^+$ and $> O^-$) and forming ion pairs with

dissolved borate. Adsorption behavior is therefore primarily modulated by the composition of the fluid, specifically the ionic strength and concentration of divalent cations. Clay mineral type seems to play a secondary role, mainly through differences in the number of accessible surface sites. The new experimental data allows us to provide a revised global characterization of sorptive boron fluxes from land to ocean, and will improve the use of boron isotopes as a proxy for critical zone proxies by constraining one of its main controls.

CRediT authorship contribution statement

Simon J. Ring: Writing – original draft, Methodology, Investigation, Formal analysis. **Michael J. Henehan:** Writing – review & editing, Supervision, Methodology, Funding acquisition, Conceptualization. **Roberts Blukis:** Writing – review & editing, Resources, Investigation. **Friedhelm von Blanckenburg:** Writing – review & editing, Supervision.

Data availability

Data are available through GFZ Data Services at https://doi.org/10.5880/GFZ.3.3.2024.003.

Declaration of competing interest

The authors declare that they have no known competing financial interests or personal relationships that could have appeared to influence the work reported in this paper.

Acknowledgements

We are grateful to Xu Zhang and two anonymous reviewers for their comments on the manuscript. We thank Paul A. Schroeder for kindly providing us with CMS IMt-2 illite. Rebecca Volkmann is thanked for performing XRD measurements on our clay samples. Misako Hatono is thanked for sharing the results of her sediment dynamics model. Alexander Balduin and Celine Sieber are thanked for their help in the lengthy pretreatment procedure of clay samples. Josefine Holtz, Jutta Schlegel and Daniel A. Frick are thanked for maintaining HELGES facilities and assisting with operation of mass spectrometers. Lastly, S.J.R. would like to thank Patrick J. Frings, Nestor Gaviria Lugo and Chenyu Wang for useful discussion during preparation of this manuscript. This research was supported by the Deutsche Forschungsgemeinschaft (DFG) Project number 455982777 awarded to M.J.H.

Appendix A. Supplementary material

Supplementary Material containing Supplementary Figures S1–S11. The supplementary figures provide additional characterization of our clay samples (Fig. S1–S6), background for our experimental set-up (Fig. S7–S8), supporting information on the adsorption of magnesium-borate ion pairs (Fig. S9–S10) and the reproducibility of our ICP-MS measurements (Fig. S11). Supplementary material to this article can be found online at https://doi.org/10.1016/j.gca.2024.08.014.

References

Borden, D., Giese, R.F., 2001. Baseline studies of the Clay Minerals Society source clays: cation exchange capacity measurements by the ammonia-electrode method. Clay Clay Miner. 49, 444–445.
Bradbury, M.H., Baeyens, B., 1997. A mechanistic description of Ni and Zn sorption on Na-montmorillonite Part II: modelling. J. Contam. Hydrol. 27, 223–248.
Bradbury, M.H., Baeyens, B., 2009. Sorption modelling on illite. Part II: actinide sorption and linear free energy relationships. Geochimica et Cosmochimica Acta 73, 1004–1013.
Chipera, S.J., Bish, D.L., 2001. Baseline studies of the Clay Minerals Society source clays: powder X-ray diffraction analyses. Clay Clay Miner. 49, 398–409.
Cividini, D., Lemarchand, D., Chabaux, F., Boutin, R., Pierret, M.-C., 2010. From biological to lithological control of the B geochemical cycle in a forest watershed (Strengbach, Vosges). Geochimica et Cosmochimica Acta 74, 3143–3163.
Cohen, S., Syvitski, J., Ashley, T., Lammers, R., Fekete, B., Li, H.-Y., 2022. Spatial trends and drivers of bedload and suspended sediment fluxes in global rivers. Water Resour. Res. 58 e2021WR031583.
Davis, J.A., Kent, D.B., 1990. Surface complexation modeling in aqueous geochemistry. In: Hochella, M.F., White, A.F. (Eds.), Mineral-Water Interface Geochemistry. Mineralogical Society of America, pp. 177–260.
Dogan, A.U., Dogan, M., Onal, M., Sarikaya, Y., Aburub, A., Wurster, D.E., 2006. Baseline studies of the Clay Minerals Society source clays: specific surface area by the Brunauer Emmett Teller (BET) method. Clay Clay Miner. 54, 62–66.
Dogan, M., Dogan, A.U., Yesilyurt, I.F., Alaygut, D., Buckner, I., Wurster, D.E., 2007. Baseline studies of the Clay Minerals Society special clays: specific surface area by the Brunauer Emmett Teller (BET) method. Clay Clay Miner. 55, 534–541.
Ercolani, C., Lemarchand, D., Dosseto, A., 2019. Insights on catchment-wide weathering regimes from boron isotopes in riverine material. Geochimica et Cosmochimica Acta 261, 35–55.
Fagel, N., 2007. Clay minerals, deep circulation and climate. Proxies in Late Cenozoic Paleoceanography 1, 139–184.
Farmer, J.R., Branson, O., Uchikawa, J., Penman, D.E., Hönisch, B., Zeebe, R.E., 2019. Boric acid and borate incorporation in inorganic calcite inferred from B/Ca, boron isotopes and surface kinetic modeling. Geochimica et Cosmochimica Acta 244, 229–247.
Foster, G.L., Pogge von Strandmann, P.A.E., Rae, J.W.B., 2010. Boron and magnesium isotopic composition of seawater. Geochemistry, Geophysics, Geosystems 11, 1–10.
Foster, G.L., Rae, J.W.B., 2016. Reconstructing ocean pH with boron isotopes in foraminifera. Annu. Rev. Earth Planet. Sci. 44, 207–237.
Gaillardet, J., Lemarchand, D., 2018. Boron in the weathering environment. In: Marschall, H., Foster, G.L. (Eds.), Boron Isotopes. Springer International Publishing AG, pp. 163–188.
Geilert, S., Vogl, J., Rosner, M., Voerkelius, S., Eichert, T., 2015. Boron isotope fractionation in bell pepper. Mass Spectrometry & Purification Techniques 1, 101.
Ghiggi, G., Humphrey, V., Seneviratne, S.I., Gudmundsson, L., 2021. G-RUN ENSEMBLE: a multi-forcing observation-based global runoff reanalysis. Water Resour. Res. 57 e2020WR028787.
Gibbs, R.J., 1977. Transport phases of transition metals in the Amazon and Yukon rivers. GSA Bull. 88, 829–843.
Goldberg, S., Forster, H.S., Heick, E.L., 1993. Boron adsorption mechanisms on oxides, clay minerals and soils inferred from ionic strength effects. Soil Sci. Soc. Am. J. 57, 704–708.
Goldberg, S., Glaubig, R.A., 1986. Boron adsorption and silicon release by the clay minerals kaolinite, montmorillonite, and illite. Soil Sci. Soc. Am. J. 50, 1442–1448.
Griffin, J.J., Windom, H., Goldberg, E.D., 1968. The distribution of clay minerals in the world ocean. Deep-Sea Res. Oceanogr. Abstr. 15, 433–459.
Gu, X., Evans, L.J., 2008. Surface complexation modelling of Cd(II), Cu(II), Ni(II), Pb(II), and Zn(II) adsorption onto kaolinite. Geochimica et Cosmochimica Acta 72, 267–276.
Gu, X., Evans, L.J., Barabash, S.J., 2010. Modeling the adsorption of Cd(II), Cu(II), Ni(II), Pb(II), and Zn(II) onto montmorillonite. Geochimica et Cosmochimica Acta 74, 5718–5728.
Hao, W., Flynn, S.L., Kashiwabara, T., Alam, M.S., Bandara, S., Swaren, L., Robbins, L.J., Alessi, D.S., Konhauser, K.O., 2019. The impact of ionic strength on the proton reactivity of clay minerals. Chem. Geol. 529, 119294.
Harriss, R.C., 1969. Boron regulation in the oceans. Nature 223, 290–291.
Hershey, J.P., Fernandez, M., Milne, P.J., Millero, F.J., 1986. The ionization of boric acid in NaCl, Na-Ca-Cl and Na-Mg-Cl solutions at 25 °C. Geochimica et Cosmochimica Acta 50, 143–148.
Hingston, F.J., 1964. Reactions between boron and clays. Aust. J. Soil Res. 2, 83–95.
Kahle, M., Stamm, C., 2007. Time and pH-dependent sorption of the veterinary antimicrobial sulfathiazole to clay minerals and ferrihydrite. Chemosphere 68, 1224–1231.
Keren, R., Gast, R.G., Bar-Yosef, B., 1981. pH-dependent boron adsorption by Na-montmorillonite. Soil Sci. Soc. Am. J. 45, 45–48.
Keren, R., Mezuman, U., 1981. Boron adsorption by clay minerals using a phenomenological equation. Clay Clay Miner. 29, 198–204.
Keren, R., Talpaz, H., 1984. Boron adsorption by montmorillonite as affected by particle size. Soil Sci. Soc. Am. J. 48, 555–559.
Klochko, K., Kaufman, A.J., Yao, W., Byrne, R.H., Tossell, J.A., 2006. Experimental measurement of boron isotope fractionation in seawater. Earth Planet. Sci. Lett. 248, 276–285.
Köhler, S., Dufaud, F., Oelkers, E.H., 2003. An experimental study of illite dissolution kinetics as a function of ph from 1.4 to 12.4 and temperature from 5 to 50 °C. Geochimica et Cosmochimica Acta 67, 3583–3594.
Lauvset, S.K., Key, R.M., Olsen, A., van Heuven, S., Velo, A., Lin, X., Schirnick, C., Kozyr, A., Tanhua, T., Hoppema, M., Jutterström, S., Steinfeldt, R., Jeansson, E., Ishii, M., Perez, F.F., Suzuki, T., Watelet, S., 2016. A new global interior ocean mapped climatology: the 1° x 1° GLODAP version 2. Earth Syst. Sci. Data 8, 325–340.
Lemarchand, D., Gaillardet, J., Lewin, É., Allègre, C.J., 2002a. Boron isotope systematics in large rivers: implications for the marine boron budget and paleo-pH reconstruction over the Cenozoic. Chem. Geol. 190, 123–140.
Lemarchand, D., Gaillardet, J., Göpel, C., Manhès, G., 2002b. An optimized procedure for boron separation and mass spectrometry analysis for river samples. Chem. Geol. 182, 323–334.

Lemarchand, D., Gaillardet, J., 2006. Transient features of the erosion of shales in the Mackenzie basin (Canada), evidences from boron isotopes. Earth Planet. Sci. Lett. 245, 174–189.
Lemarchand, E., Schott, J., Gaillardet, J., 2005. Boron isotopic fractionation related to boron sorption on humic acid and the structure of surface complexes formed. Geochimica et Cosmochimica Acta 69, 3519–3533.
Lemarchand, E., Schott, J., Gaillardet, J., 2007. How surface complexes impact boron isotope fractionation: evidence from Fr and Mn oxides sorption experiments. Earth Planet. Sci. Lett. 260, 277–296.
Li, L., Ni, J., Chang, F., Yue, Y., Frolova, N., Magritsky, D., Borthwick, A.G.L., Ciais, P., Wang, Y., Zheng, C., Walling, D.E., 2020. Global trends in water and sediment fluxes of the world's large rivers. Science Bulletin 65, 62–69.
Liu, Y., Alessi, D.S., Flynn, S.L., Samrat Alam, M., Hao, W., Gingras, M., Zhao, H., Konhauser, K.O., 2018. Acid-base properties of kaolinite, montmorillonite and illite at marine ionic strength. Chem. Geol. 483, 191–200.
Liu, Y.-C., You, C.-F., Huang, K.-F., Wang, R.-M., Chung, C.-H., Liu, H.-C., 2012. Boron sources and transport mechanisms in river waters collected from southwestern Taiwan: isotopic evidence. J. Asian Earth Sci. 58, 16–23.
Lu, S., Dosseto, A., Lemarchand, D., 2024. Boron in wildfires: new insights into boron isotope fractionation during volatilisation, leaching and adsorption after combustion. Geochimica et Cosmochimica Acta 379, 208–218.
Mao, H.-R., Liu, C.-Q., Zhao, Z.-Q., 2019. Source and evolution of dissolved boron in rivers: insights from boron isotope signatures of end-members and model of boron isotopes during weathering processes. Earth Sci. Rev. 190, 439–459.
Mattigod, S.V., Frampton, J.A., Lim, C.H., 1985. Effect of ion-pair formation on boron adsorption by kaolinite. Clay Clay Miner. 33, 433–437.
Mezuman, U., Keren, R., 1981. Boron adsorption by soils using a phenomenological adsorption equation. Soil Sci. Soc. Am. J. 45, 722–726.
Millero, F.J., 2013. Chemical Oceanography. CRC Press.
Millero, F.J., Feistel, R., Wright, D.G., McDougall, T.J., 2008. The composition of standard seawater and the definition of the reference-composition salinity scale. Deep Sea Res. Part I 55, 50–72.
Motta, M.M., Miranda, C.F., 1989. Molybdate adsorption on kaolinite, montmorillonite, and illite: constant capacitance modeling. Soil Sci. Soc. Am. J. 53, 380–385.
Müller, G., Middelburg, J.J., Sluijs, A., 2021. Introducing GloRiSe – a global database on river sediment composition. Earth Syst. Sci. Data 13, 3565–3575.
Nir, O., Vengosh, A., Harkness, J.S., Dwyer, G.S., Lahav, O., 2015. Direct measurement of the boron isotope fractionation factor: reducing the uuncertainty in reconstructing ocean paleo-pH. Earth Planet. Sci. Lett. 414, 1–5.
Noireaux, J., Sullivan, P.L., Gaillardet, J., Louvat, P., Steinhoefel, G., Brantley, S.L., 2021. Developing boron isotopes to elucidate shale weathering in the critical zone. Chem. Geol. 559, 119900.
Palmer, M.R., Spivack, A.J., Edmond, J.M., 1987. Temperature and pH controls over isotopic fractionation during adsorption of boron on marine clay. Geochimica et Cosmochimica Acta 51, 2319–2323.
Parkhurst D. L. and Appelo C. A. J. (2013). Description of input and examples for PHREEQC version 3, U.S. Geologic Survey Techniques and Methods, Book 6 (U.S. Geological Survey, Denver, CO).
Poppe, L.J., Paskevich, V.F., Hathaway, J.C., Blackwood, D.S., 2001. Separation of the silt and clay fractions for X-ray powder diffraction by centrifugation. U.S. Geol. Surv. Open File Rep. 01–041.
Roux, P., Lemarchand, D., Redon, P.-O., Turpault, M.-P., 2022. B and $\delta^{11}B$ biogeochemical cycle in a beech forest developed on a calcareous soil: pools, fluxes, and forcing parameters. Sci. Total Environ. 806, 150396.
Schlesinger, W.H., Vengosh, A., 2016. Global boron cycle in the Anthropocene. Global Biogeochem. Cycles 30, 219–230.
Schwarcz, H.P., Agyei, E.K., McMullen, C.C., 1969. Boron isotopic fractionation during clay adsorption from sea-water. Earth Planet. Sci. Lett. 6, 1–5.
Simon, L., Lécuyer, C., Maréchal, C., Coltice, N., 2006. Modelling the geochemical cycle of boron: implications for the long-term $\delta^{11}B$ evolution of seawater and oceanic crust. Chem. Geol. 225, 61–76.
Spivack, A.J., Palmer, M.R., Edmond, J.M., 1987. The sedimentary cycle of boron isotopes. Geochemica et Cosmochimica Acta 51, 1939–1949.
Stewart, J.A., Christopher, S.J., Kucklick, J.R., Bordier, L., Chalk, T.B., Dapoigny, A., Douville, E., Foster, G.L., Gray, W.R., Greenop, R., Gutjahr, M., Hemsing, F., Henehan, M.J., Holdship, P., Hsieh, Y.-T., Kolevica, A., Lin, Y.-P., Mawbey, E.M., Rae, J.W.B., Robinson, L.F., Shuttleworth, R., You, C.-F., Zhang, S., Day, R.D., 2020. NIST RM 8301 boron isotopes in marine carbonate (simulated coral and foraminifera solutions): inter-laboratory $\delta^{11}B$ and trace element ratio value assignment. Geostandards and Geoanalytical Research 45, 77–96.
Su, C., Suarez, D.L., 1995. Coordination of adsorbed boron: a FTIR spectroscopic study. Environ. Sci. Tech. 29, 302–311.
Syvitski, J., Ángel, J.R., Saito, Y., Overeem, I., Vörösmarty, C.J., Wang, H., Olago, D., 2022. Earth's sediment cycle during the Anthropocene. Nature Reviews Earth & Environment 3, 179–196.
Tertre, E., Castet, S., Berger, G., Loubet, M., Giffaut, E., 2006. Surface chemistry of kaolinite and Na-montmorillonite in aqueous electrolyte solutions at 25 and 60°C: experimental and modeling study. Geochemica et Cosmochimica Acta 70, 4579–4599.
Totten, M.W., Hanan, M.A., Knight, D., Borges, J., 2002. Characteristics of mixed-layer smectite/illite density separates during burial diagenesis. Am. Mineral. 87, 1571–1579.
Vogl, J., Rosner, M., 2011. Production and certification of a unique set of isotope and delta reference materials for boron isotope determination in geochemical, environmental and industrial materials. Geostand. Geoanal. Res. 36, 161–175.
Xiao, J., Vogl, J., Rosner, M., Jin, Z., 2022. Boron isotope fractionation in soil-plant systems and its influence on biogeochemical cycling. Chem. Geol. 606, 120972.
Yin, X., Liu, F., Liu, Q., Zhang, Y., Gao, C., Zhang, S., Ridley, M.K., Liu, Y., 2023. Boron isotope fractionation between $B(OH)_3$ and $B(OH)_4^-$ in aqueous solutions: a theoretical investigation beyond the harmonic and Born-Oppenheimer approximations. Chem. Geol. 627, 121455.
Zhang, X., Saldi, G.D., Schott, J., Bouchez, J., Kuessner, M., Montouillout, V., Henehan, M., Gaillardet, J., 2021. Experimental constraints on Li isotope fractionation during the interaction between kaolinite and seawater. Geochimica et Cosmochimica Acta 292, 333–347.